AIP Journal of Applied Physics

Surface effects on the optical and photocatalytic properties of graphene-like ZnO:Eu3+ nanosheets

Lili Yang, Zhe Wang, Zhiqiang Zhang, Yunfei Sun, Ming Gao, Jinghai Yang, and Yongsheng Yan

Citation: Journal of Applied Physics **113**, 033514 (2013); doi: 10.1063/1.4776225
View online: http://dx.doi.org/10.1063/1.4776225
View Table of Contents: http://scitation.aip.org/content/aip/journal/jap/113/3?ver=pdfcov
Published by the AIP Publishing

Surface effects on the optical and photocatalytic properties of graphene-like ZnO:Eu^{3+} nanosheets

Lili Yang,[1,2,3,a)] Zhe Wang,[1,3] Zhiqiang Zhang,[1,3] Yunfei Sun,[4] Ming Gao,[1,3,4] Jinghai Yang,[1,3,a)] and Yongsheng Yan[2]
[1]*Institute of Condensed State Physics, Jilin Normal University, Siping 136000, China*
[2]*Institute of Chemistry and Chemical Engineering, Jiangsu University, Zhenjiang 212013, China*
[3]*Key Laboratory of Functional Materials Physics and Chemistry (Jilin Normal University), Ministry of Education, Siping 136000, China*
[4]*Key Laboratory of Excited State Physics, Changchun Institute of Optics Fine Mechanics and Physics, Chinese Academy of Sciences, Changchun 130033, China*

(Received 29 September 2012; accepted 28 December 2012; published online 17 January 2013)

The graphene-like ZnO:Eu^{3+} (ZEO) nanosheets with different Eu^{3+} doping concentrations are synthesized successfully by a simple hydrothermal method. We utilize the native surface effect in the ZEO nanosheets for the first time to certify the resonant energy transfer mechanism from the ZnO host to the Eu^{3+} ions by means of the power-dependent photoluminescence technique. Meanwhile, to further explore the functional applications of the graphene-like ZEO, we also characterize their photocatalytic activity on the Rhodamine B dye and reveal that both the higher specific surface area and Eu^{3+} doping lead to the higher degradation efficiency of ZEO nanosheets.
 [http://dx.doi.org/10.1063/1.4776225]

I. INTRODUCTION

Doping is an effective way to change the optical and electrical properties of semiconductor materials or further improve the performance of their optoelectronic devices. Rare earth (RE) elements such as Eu, Er, and Tb are the famous visible luminescence centers once they are incorporated into the host matrix. Therefore, people expect that doping RE element into the lattices of ZnO would provide the efficient visible light emissions.[1–5] Recently, Eu^{3+} as one of the most famous red emitting activators has been successfully incorporated into the ZnO nanoparticles, nanorods arrays, and nanospheres, and most of them provide the red emission at 615 nm due to the intra-4f shell $^5D_0$-$^7F_2$ transition, which makes ZnO:Eu^{3+} (ZEO) turn into a promising candidate for the white light-emitting diode and planar display due to their multicolor emissions.[1,6,7] However, rare work has been reported about the Eu^{3+}-doped ZnO nanosheets, especially for the very thin and soft nanosheets as metaphorically called the graphene-like,[8] since it is a huge challenge to incorporate the Eu ions into the ZnO lattices due to the giant differences in ionic radius and charge between Zn^{2+} and Eu^{3+} ions.

Recently, especially after the emergence of graphene, the nanosheets obtained by the delamination of layered compounds have been recognized as a novel class of nanostructured materials due to their unique structural feature of ultimate two-dimensional anisotropy with extremely small thickness in nanometer.[8–12] From fundamental point of view, this extremely small thickness with huge surface will definitely bring the surface effects into the optical properties due to their much higher specific surface area. In our previous work about Eu^{3+} doped ZnO nanowires, we already pointed out that ZnO host resonantly transferred their energy to Eu^{3+} via the oxygen vacancy as trapping and energy storage centers.[3] Then, how will the strong surface effects influence the Eu^{3+} emission once Eu^{3+} is doped into the graphene-like ZnO nanosheets? To help reveal this deep fundamental physical phenomenon, we need to utilize the excitation power-dependent photoluminescence (PL) technique, since it is an effective method to gain a good understanding and systematically investigate the luminescence mechanism and the excitation pathways of the RE^{3+} ions in semiconductor hosts.[13–15] However, the excitation power-dependent PL for the Eu^{3+} doped ZnO nanostructures is rarely reported.

Therefore, in this paper, we would like to present the controllable synthesis of graphene-like ZnO:Eu^{3+} nanosheets by a hydrothermal method. The surface effects on their optical properties, especially the energy transfer mechanism from ZnO host to Eu^{3+} ions, and photocatalytic activities will be investigated in detail.

II. EXPERIMENTAL SECTION

A. Synthesis

Eu-doped ZnO nanosheets were synthesized via the hydrothermal method with post-annealing treatment. $Zn(NO_3)_2{\cdot}6H_2O$ was first dissolved in the deionized water. Eu_2O_3 powder was dissolved in dilute nitric acid to obtain a 0.05 mol/l aqueous solution of europium nitrate. The above two solutions were mixed together, in which the concentration of the metal ions was adjusted to 0.05 mol/l. Then the urea was added into it with a Zn:Eu:urea molar ratio of 1:0.02:2, 1:0.02:4, and 1:0.02:8, respectively. After stirring, the solution was transferred into a 100 ml teflon-lined autoclave, which was filled to nearly its 80% capacity. The autoclave was kept in a dry cabinet at 120 °C for 6 h, then the

[a)]Authors to whom correspondence should be addressed. Electronic addresses: llyang@jlnu.edu.cn and jhyang1@jlnu.edu.cn.

solution was cooled down to room temperature and washed with alcohol and deionized water for three times. After dried at 60 °C, the powder was annealed at 400 °C in air for 2 h. Herein, we obtain the as-grown samples named as ZEO-2, ZEO-4, ZEO-8 according to the content of urea, respectively. For comparison, we also prepared the undoped ZnO sample in the similar process only without adding Eu^{3+} solution, which was named as UZO.

B. Characterization

X-ray diffraction (XRD) patterns were recorded by a MAC Science MXP-18 X-ray diffractometer using a Cu target radiation source was used to study the crystal structure and morphology of the samples. The scanning electron microscope (SEM, S-570, Hitachi) with an energy dispersive spectrometer (EDS) was used to characterize the morphology and different chemical composition of the samples. The transmission electron microscope (TEM, JEM-2100, JEOL) spectroscopy system was used to qualitatively confirm the detailed microscopic structure. A quantitative compositional analysis was carried out by using an X-ray photoelectron spectroscopy (XPS) in an ultra-high vacuum chamber at a pressure lower than 1.333×10^{-7} Pa. The PL measurements were performed on the Renishaw invia spectroscopy excited by a continuous He-Cd laser with a wavelength of 325 nm.

C. Photocatalytic activity measurement

Photocatalytic activity of the samples was determined by the degradation of Rhodamine B (RhB) under UV light irradiation. Photoirradiation was carried out using a 250-W high-pressure Hg lamp (centered at 365 nm). Before exposure to UV irradiation, the mixed aqueous solutions of RhB and as-synthesized products were magnetically stirred thoroughly in the dark until reaching the adsorption equilibrium of the RhB on the catalyst. After different irradiation intervals, the solution concentration of RhB was analyzed by a UV-vis spectrophotometer (UV-5800PC, Shanghai Metash Instruments Co., Ltd) at room temperature. In addition, commercial ZnO nanoparticles powders (25–40 nm in size, Shanghai Chemical Reagent Co., Ltd) were adopted for reference catalysts to compare the photocatalytic activity under the same experimental conditions.

III. RESULTS AND DISCUSSION

A. Microstructure and morphology

Fig. 1 shows the XRD patterns of the as-prepared ZnO and ZnO:Eu^{3+} samples. We can see that all the diffraction peaks can be indexed to wurtzite-type ZnO structure for all the samples according to the standard JCPDS 36-1451 file for ZnO. For ZnO:Eu^{3+} samples, no diffraction peaks are detected from europium oxides or any other impurities, which indicates that Eu^{3+} ions are successfully doped into the crystal lattice of ZnO matrix. We can also find in Fig. 1 that, with increasing the urea content, the diffraction intensities in the XRD patterns decrease step by step, indicating the degeneration of crystalline qualities. Hence, we can deduce that the Eu^{3+} doping concentration in ZnO probably

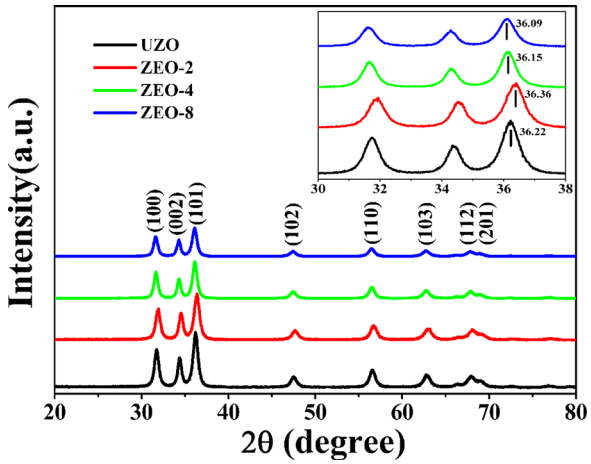

FIG. 1. XRD patterns of UZO, ZEO-2, ZEO-4, and ZEO-8. The inset shows the magnified patterns in the vicinity of 30° ~ 40°.

increases with the increase of urea content, which will be further proved by the SEM results. Generally, as the ionic radius of Eu^{3+} is much bigger than that of Zn^{2+}, the incorporation of Eu^{3+} ions into the ZnO matrix necessarily leads to the expansion of the unit-cell volume of the ZnO:Eu^{3+} samples, which will result in the shift of diffraction peaks to the lower angle. However, as shown in the inset of Fig. 1, in comparison with the XRD pattern of UZO, we can find that the diffraction peak positions first shift to the higher angle for ZEO-2 and then shift to the lower angle again for ZEO-4 and ZEO-8, indicating that the Eu^{3+} doping first makes the lattice shrink and then expand again. This phenomenon may be explained as follows: First, the incorporated Eu^{3+} ions probably build the obstructions for the movement of grain boundary and limit the grain growth in ZnO, thus the lattice of ZEO-2 sample shrinks.[16–18] However, once the Eu^{3+} concentration increases in ZEO-4 and ZEO-8, the lattice expands again since the Eu^{3+} ions incorporated into the ZnO lattices necessarily lead to the expansion of the unit-cell volume of the ZnO:Eu^{3+} samples as the ionic radius of Eu^{3+} is much bigger than that of Zn^{2+}.

Fig. 2 presents the SEM images of the UZO and ZnO:Eu^{3+} samples. All the samples own nanoflake morphologies. As shown in Fig. 2(a), the thickness of UZO nanoflake is about 200 nm. While, Figs. 2(b)–2(d) illustrated the thickness of ZEO-2, ZEO-4, and ZEO-8 nanoflakes is 80 nm, 100 nm, and 150 nm, respectively.

We further performed the EDS measurement on the nanosheets to verify the chemical composition of these nanoflakes, which has been shown in Fig. 3. In Figure 3(a), only Zn and O elements can be detected in UZO sample. While, in Figures 3(b)–3(d), we can find that, except the Zn and O elements, a small amount of Eu elements exist in the ZEO-2, ZEO-4, and ZEO-8 samples. The corresponding quantitative concentration of Eu^{3+} has been estimated to be 1.03%, 1.39%, 1.98%, respectively, which strongly confirms the deduction from XRD results. In addition, since the Eu^{3+} concentration in the initial solution is fixed and only urea content increases step by step. Therefore, we can deduce that urea content in initial growth solution may promote the incorporation of Eu^{3+} ions into ZnO.

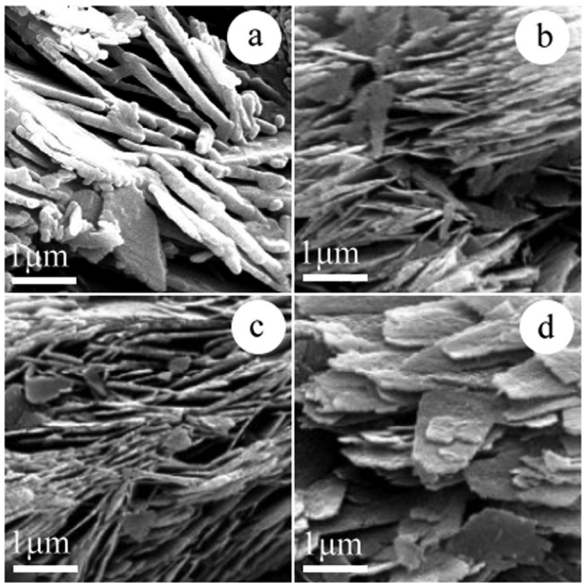

FIG. 2. SEM images of UZO (a), ZEO-2 (b), ZEO-4 (c), and ZEO-8 (d).

To qualitatively reveal the detailed microscopic structure, the TEM image of ZEO-8 was presented in Fig. 4. We can see in Fig. 4(a) that the copper substrate is covered with a layer of large-area, continuous, crumpled and very thin sheet, which is quite similar to the graphene sheet.[19,20] The rumpling mainly comes from the sonication and sheet take-out process. To make the structure clearly, the high magnification TEM images corresponding to the R1 and R2 parts marked by the red dot rings in Fig. 4(a) were shown in Figs. 4(b) and 4(d), respectively. R1 mainly focused on the wrinkle of the sheets, while R2 was taken at the edge of the sheets. The HRTEM image corresponding to one of the wrinkle place marked by the red dot ring in Fig. 4(b) was illustrated in Fig. 4(c). We can clearly see the fringe lines along at least three directions, which have been marked by the red, green, and blue lines in the images. The fringe lines along the red and blue arrow directions finally crossed with each other due to the formation of wrinkles. The fringe spaces for three directions are all 0.268 nm, which is corresponding to the (002) plane distance of the standard wurtzite-type ZnO structure (cell constants of $a = 3.249$ Å and $c = 5.206$ Å). However, this spacing is bigger than that of standard ZnO, which is mainly caused by the cell volume expansion when the Eu^{3+} ions doped into ZnO. From the red dot rectangle part in Fig. 4(d), we can see that the nanosheet can be distinguished as single-layer or double-layers. The HRTEM image corresponding to the places marked by the small red and blue dot rectangles in Fig. 4(d) was illustrated in Figs. 4(e) and 4(f). The fringe spaces are all estimated to be 0.268 nm, which have a great agreement with that in Fig. 4(c). However, we can clearly see the defects cross the fringes in Fig. 4(e) as marked by the red dot rectangles, which maybe caused by the Eu^{3+} incorporation into the ZnO lattices.

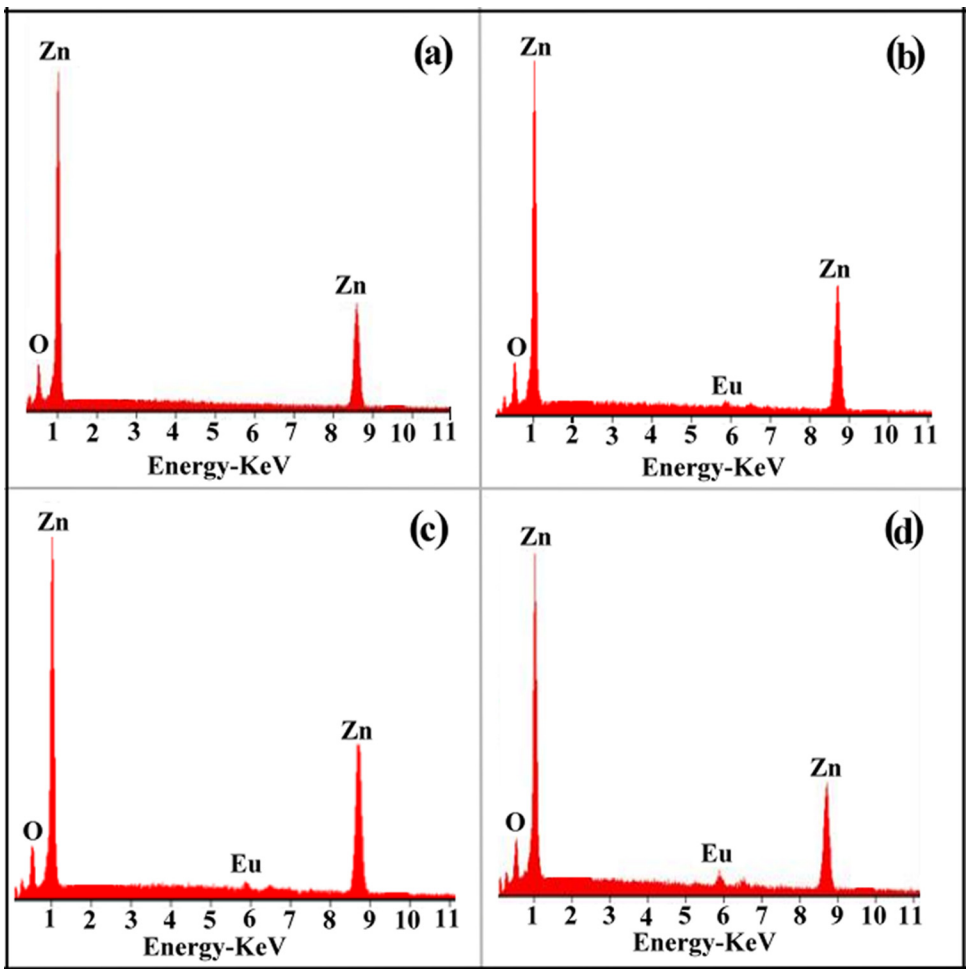

FIG. 3. EDS spectra of UZO (a), ZEO-2 (b), ZEO-4 (c), and ZEO-8 (d).

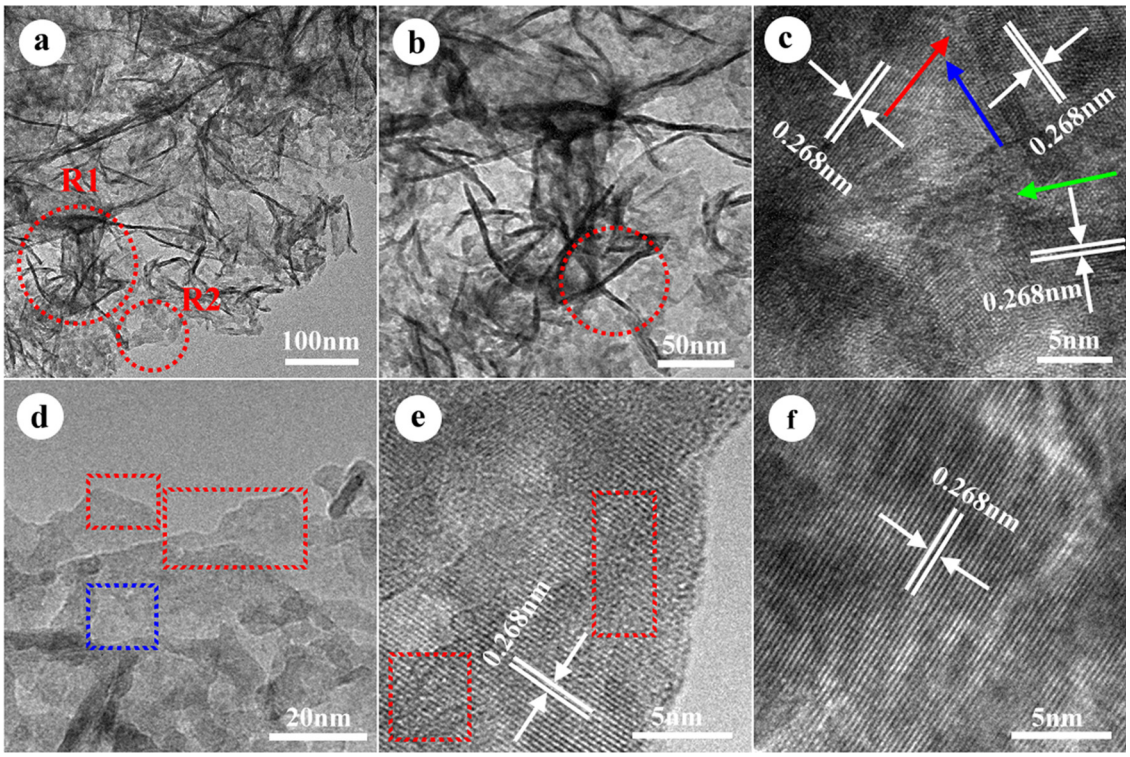

FIG. 4. TEM and HRTEM images of ZEO-8. (a) TEM image; (b) high-magnification TEM image corresponding to the wrinkle region marked by red dot ring (R1) in (a); (c) HRTEM image corresponding to the region marked by the red dot ring in (b); (d) high-magnification TEM image corresponding to the edge region marked by red dot ring (R2) in (a); (e) HRTEM image corresponding to the region marked by the small red dot rectangle in (d); (f) HRTEM image corresponding to the region marked by the blue dot rectangle in (d).

To further investigate the chemical composition and the bonding state in the graphene-like ZnO:Eu^{3+} nanosheets, we performed XPS measurements on the ZEO-8 sample. Prior to the XPS measurements, the sample was cleaned by sputtering with an Ar ion beam to remove any potential surface contamination. As shown in Fig. 5(a), the typical XPS survey scan confirms the presence of Zn, O, Eu, and C elements, indicating that no other impurities exist in ZEO-8 sample.

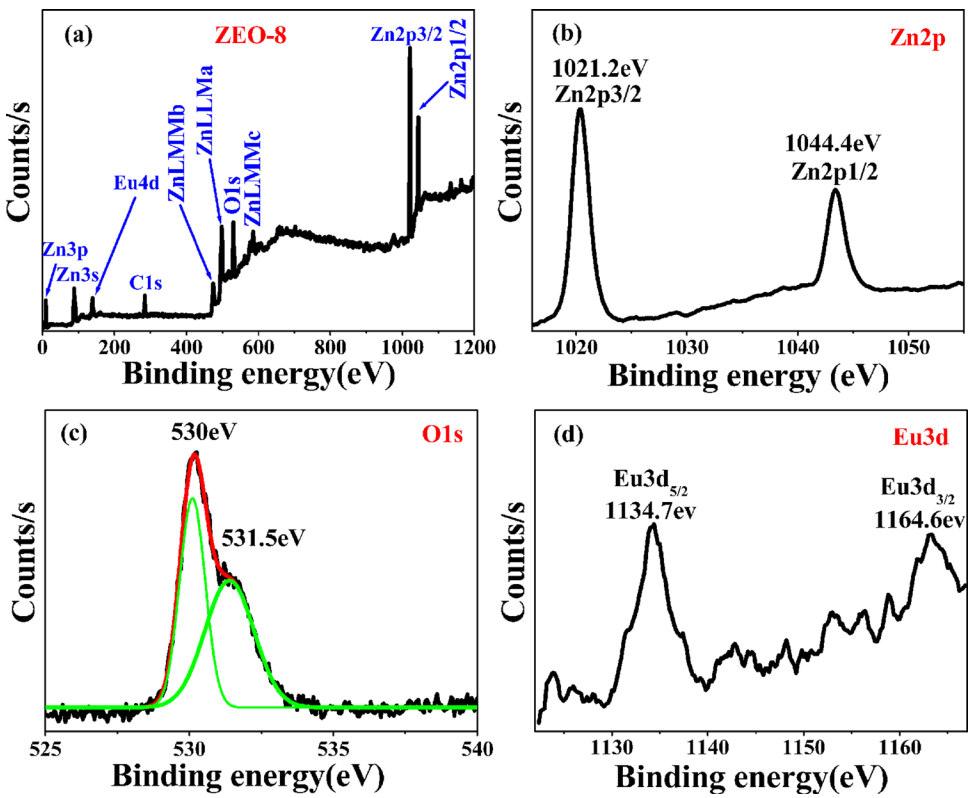

FIG. 5. XPS spectrum of ZEO-8. (a) XPS survey spectrum; (b) Zn 2p3/2 and Zn 2p1/2 XPS spectrum; (c) O1s XPS spectrum where two components (green curves) were used to deconvolute the experimental peak; (d) Eu 3d5/2 and Eu 3d3/2 XPS spectrum.

We would like to mention that, for all the XPS spectra in Fig. 5, the binding energies have been calibrated by taking the carbon C1s peak (285.0 eV) as reference. The high resolution scans of Zn2p, O1s, and Eu3d of ZEO-8 are shown in Figs. 5(b)–5(d). In Fig. 5(b), the peaks located at 1021.2 and 1044.4 eV are associated to $Zn2p_{3/2}$ and $Zn2p_{1/2}$, respectively.[21–24] Since the O1s XPS spectrum in Fig. 5(c) is obviously unsymmetric, we use Gaussian function to fit it and the deconvolutions show the presence of two different O1s peaks. The peak centered at 531.0 eV is associated to the O^{2-} ion in the wurtzite structure surrounded by the Zn atoms with their full complement of nearest-neighbor O^{2-} ions,[21–24] whereas the peak centered at 531.5 eV can be ascribed by many authors to the presence of OH bonds, i.e., ZnO(OH).[21–24] Fig. 5(d) presents the Eu3d XPS spectra of ZEO-8. The two characteristic peaks at 1164.6 and 1134.7 eV are attributable to the core levels of $Eu3d_{3/2}$ and Eu $3d_{5/2}$, respectively, which indicates that the Eu ions are trivalent.[25,26] By fitting the integrated peak areas and using the calibrated atomic sensitivity factors, the atomic ratio of Eu to Zn was quantitatively determined to be 1.96%, which is well consistent with the EDS results.

B. Photoluminescent properties and energy-transfer mechanisms

Fig. 6(a) shows the room-temperature PL spectra of the as-prepared ZnO, ZEO-2, ZEO-4, and ZEO-8. All the spectra consist of an UV peak at 386 nm and a green emission peak at about 550 nm. Usually, the green emission is related to the oxygen vacancy (*V*o), which is attributed to the transition between the electron close to the conduction band and deeply trapped hole at *V*o centre (oxygen vacancy containing no electrons)[27–29] or the transition between the electron at Vo^{+} (with one electron) or Vo^{++} (with two electrons) and the hole at vacancy associated with the surface defects.[29,30] The UV emission band is related to a near band-edge (NBE) transition of ZnO, namely, the recombination of the free excitons (376 nm). The room temperature PL peak position can be different, for example, the transition energy from 375 nm (Ref. 31) to 383 nm,[32] and the exact energy position depends on the contribution between the free exciton and the transition between free electrons to acceptor bound holes.[33–37] In our case, the UV emission peak of UZO located at 386 nm, which exhibits an obvious redshift in comparison with other ZnO nanostructures and bulk materials.[31–37] We would like to propose that this redshift is related to the surface band bending effect due to the graphene-like morphologies with large surface-to-volume ratio.

The as-synthesized ZnO nanostructures are usually n-type, but both donor-and acceptor-like states are present within the band gap.[38] Hence, some donor electrons in the conduction band will reduce their energy by occupying the acceptor-like surface states. A negative surface charge is generated, counterbalanced by a positive space charge that originates from ionized donors within a depletion width d away from the surface, so that overall charge neutrality is maintained. Consequently, a built-in electric filed and the corresponding electrostatic potential will built up so that the

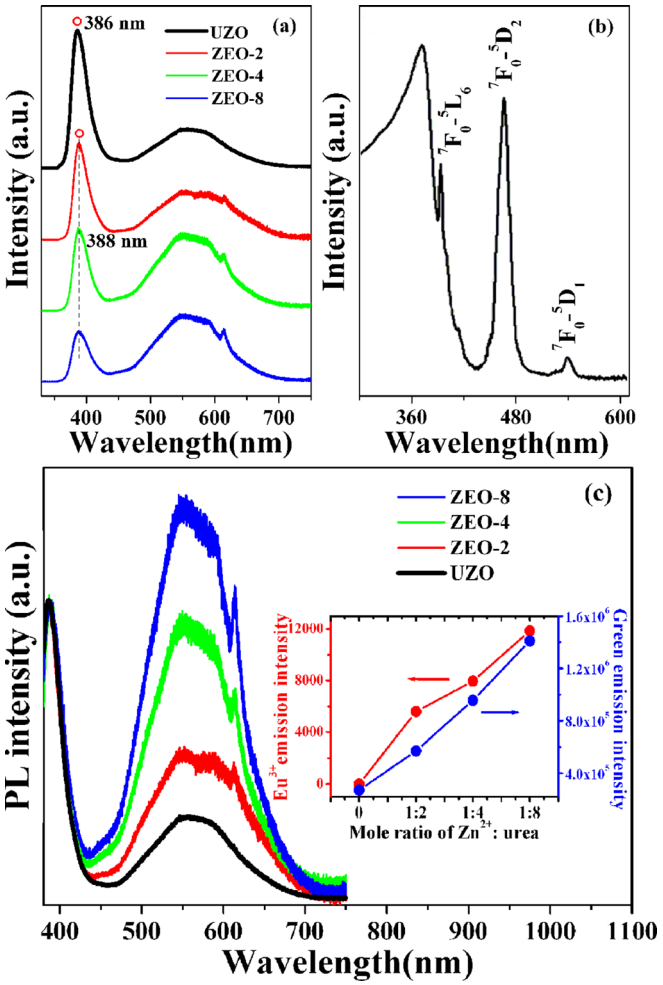

FIG. 6. (a) Room temperature PL spectra of UZO, ZEO-2, ZEO-4, and ZEO-8; (b)excitation spectrum of ZEO-8; (c) visible light region of PL spectra with UV peak normalization; the inset illustrates the intensities of both green and red emissions via the mole ratio of Zn^{2+}:urea.

energy bands bend upwards as they approach the surface and finally results in a surface depletion layer, which will strongly influence the PL properties of ZnO nanostructures.[39–44] We can simply estimate band-bending effect and its impact on PL of ZnO and ZnO:Eu^{3+} samples in detail. The width of the surface depletion region can be described as[44,45]

$$d = \left[\frac{2\varepsilon_{ZnO}\varepsilon_0\Phi_S}{e^2 N_D^+(T)}\right]^{1/2}, \quad (1)$$

where ε_{ZnO} is the relative dielectric constant of ZnO, ε_0 is the permittivity of vacuum, Φ_S is the height of potential barrier, e is the electronic charge, and $N_D^+(T)$ is the temperature dependent activated donor concentration, which can be described as follows:

$$N_D^+(T) = \frac{N_D}{1 + 2\exp\left(\frac{E_F - E_D}{k_B T}\right)}. \quad (2)$$

Using $N_D^+(T) \sim 10^{17}\,\mathrm{cm}^{-3}$ at room temperature, $\varepsilon_{ZnO} \sim 8.7$, and Φ_S is of the order of 0.5 eV,[43] the calculated width of depletion region is ~69 nm. Since the thickness of UZO and ZEO samples in our case is obviously thin, which is far

smaller than 69 nm as shown in Fig. 4, they should be thoroughly depleted. Hence, the strong upward band bending near surface will play an important role to influence their PL properties, which will finally result in the redshift of their UV emission compared to other ZnO nanostructures and bulk materials. Furthermore, in Fig. 6(a), we can also observe that the Eu^{3+} doping leads further red shift of the UV emission (388 nm) in comparison with the UZO samples. Since the change of Eu^{3+} doping concentration has no influence on the UV emission peak position as shown by the black dot line in Fig. 6(a), this further redshift maybe attributed to the further thickness decrease of the graphene-like ZnO:Eu^{3+} nanosheets as discussed in the SEM results of Fig. 2, which leads to a further stronger surface band bending.

Besides the UV and green emission band in the PL spectra of ZnO:Eu^{3+} nanosheets in Fig. 6(a), we can also observe an additional red emission peak centered at ~613 nm, which can be attributed to the intra-4f transition of Eu^{3+} ions, in particular, the $^5D_0$–$^7F_2$ transition.[1–3,6,7,46] In our previous work, we revealed the mechanism of Eu^{3+} emission in the ZnO nanowire arrays, i.e., a resonant energy transfer from the ZnO host to the Eu^{3+} ions via the *Vo* as trapping and energy storage centers.[3] Fig. 6(b) presents the excitation spectra of ZEO-8 with monitoring 613 nm emission. The excitation peaks at 393, 465, and 538 nm are likely originated from the $^7F_0$-$^5L_6$ and $^7F_0$-^5D_J (J = 2, 1) transition of Eu^{3+} ions.[47,48] In addition, it is obvious to see that a strong excitation peak appears at UV range that corresponds to the NBE transition of ZnO, which further confirms the energy transfer from UV-generated delocalized electron and hole pairs in ZnO host to Eu^{3+} ions.[47,48] We further normalized the UV emission to compare the green and red emissions in the PL spectra as shown in Fig. 6(c) and summarized their intensities via the mole ratio of Zn^{2+}:urea in the inset of Fig. 6(c). Obviously, the intensities of both green emission caused by Vo and red emission from Eu^{3+} ions increase step by step with increasing the urea content in the growth solution. Since the increase of urea content will cause the increase of the Eu^{3+} doping concentration in ZnO nanosheets as discussed in the XRD results, two effects will be appeared. On one hand, the red emission from Eu^{3+} ions will increase step by step; on the other hand, the Vo density will increase in the samples due to a higher valence Eu^{3+} ions replace a lower valence Zn^{2+} ions.[49] As a result, the green emission will be enhanced as well. Moreover, the same variation tendency for both emissions further confirms their native relationship, i.e., Vo indeed serves as the trapping and energy storage centers for the resonant energy transfer from the ZnO host to the Eu^{3+} ions in our case. The detailed schematic illustration of energy transfer mechanism can be found in Fig. 7(a). Due to the surface effects, the conduction band (CB), valence band (VB), and the defect levels are up-bending. The probable Eu^{3+} emission mechanism can be described as follows: A large amount of carriers are excited from the VB to CB of ZnO. Then, they are trapped at energy storage centers of *Vo*. By means of a resonant energy transfer process, the trapped carriers at the *Vo* could transfer their energy to the Eu^{3+} subsystem (i.e., $^7F_0 \rightarrow {}^5D_2$). As a final step of the energetic process, Eu^{3+} ions go through the radiative transition from $^5D_0$ to $^7F_2$, giving out the red emission.

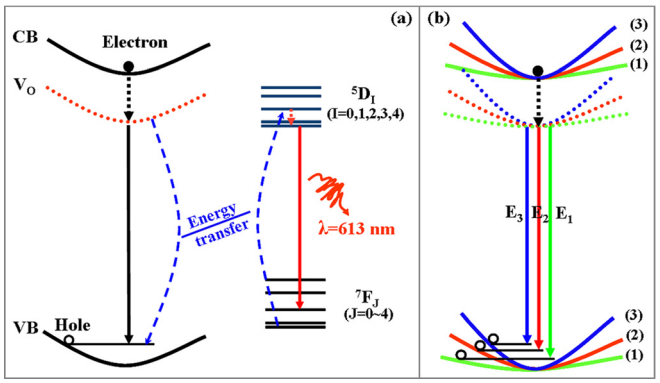

FIG. 7. (a) Schematic illustrating the proposed mechanism of energy transfer from the ZnO host to the Eu^{3+} ions. The dashed and the solid lines with arrows represent nonradiative and radiative processes, respectively; (b) schematic illustrating the proposed variation of energy transfer process with different power excitation.

The excitation power-dependent photoluminescence is an effective method to systematically investigate the photoluminescence mechanism and the excitation pathways of the Eu^{3+} ions in semiconductor hosts. Therefore, we performed the excitation power-dependent PL measurement on ZEO-8 sample and their spectra are shown in Fig. 8. To analyze, the UV peak position, red and green emission intensity via the normalized excitation power density is summarized in Fig. 9. Obviously, as shown in Figs. 8 and 9, not only the UV peak position keeps red-shift with increasing excitation power[50,51] but also the red and green emission intensity initially enhances with the increase in excitation power up to around 0.4 mW and 2 mW, respectively, and then decreases again.[50] In our case, with increasing the excitation power, more and more photo-generated electrons will be formed in the graphene-like ZEO-8 samples, so that the Fermi level will move upward to the conductive band and lead to the further upward band bending, which finally results in the continued red-shift of UV position.[52] Simultaneously, the *Vo* states will trap more and more photo-generated electrons and cause the initially enhancement of green emission. However, the number of *Vo* states is limited after all. When all the *Vo* states

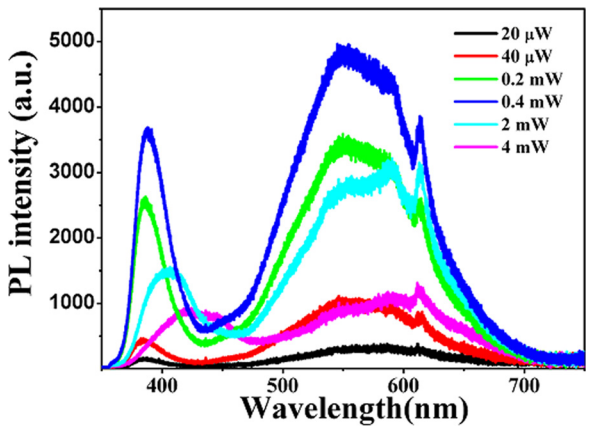

FIG. 8. Excitation power dependence of the room-temperature PL spectra of ZEO-8.

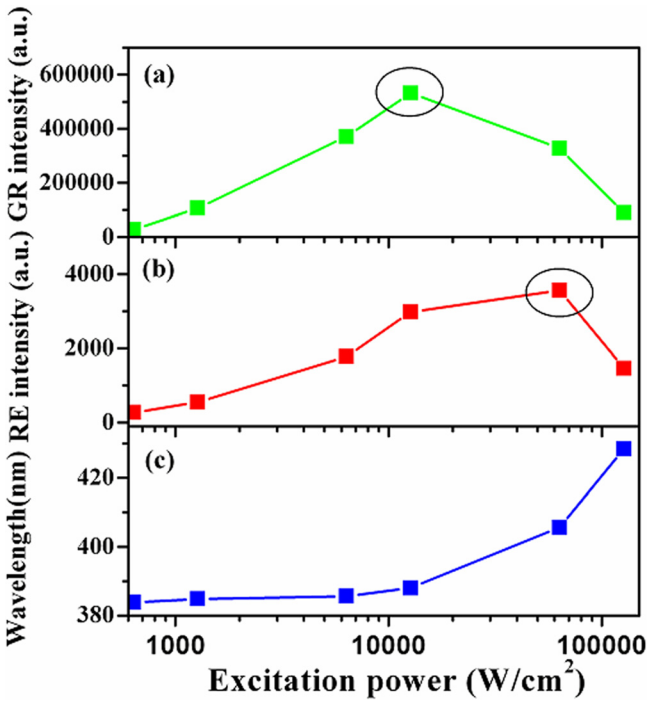

FIG. 9. Green (a) and red (b) emission intensities and UV wavelength (c) as a function of excitation power density.

have been occupied by the electrons, the green emission reaches the maximum, which corresponds to the situation with the excitation power of 0.4 mW in our case as shown in Fig. 9(a). Above this excitation power, the competition between green emission and nonradiative recombination pathway turns out to be violent so that the green emission intensity falls off.[50,51] Due to the native relationship between green and red emissions mentioned above, their intensity should reach the maximum at the same excitation power. However, we can see from Fig. 9(b) that the intensity of red emission keeps increasing when the green emission intensity falls off after 0.4 mW and finally turns into the maximum when the excitation power is 2 mW. Therefore, we would like to propose that, due to the high specific surface area in the graphene-like ZEO-8 sample, the adjustment of band alignment during the increase process of excitation power also has a strong influence on the resonant energy transfer from the ZnO host to the Eu^{3+} ions.[50,51] As illustrated in Fig. 7(b), with the increase of excitation power, the energy band keeps upward bending as marked by (1), (2), and (3). The corresponding energy difference (E) between Vo and valance band can be assigned to E_1, E_2, and E_3, respectively, which follows the relationship of $E_1 > E_2 > E_3$. In that case the resonant energy transfer is allowed; it is reasonable to believe that a critical E exists, for example, E_2 in our case, which is in well agreement with the energy of $^7F_0 \rightarrow {}^5D_2$ and quite favorable for the resonant energy transfer to make the intensity of Eu^{3+} red emission reach the maximum. For the region of $E < E_2$, the intensity of Eu^{3+} red emission will be enhanced step by step with the increase of the excitation power since the energy is near to the resonant critical energy step by step. While, once in the case of $E > E_2$, the efficiency of resonant energy transfer will be lower again since the energy does not match well again. Thus, the intensity of Eu^{3+} red emission turns weak.

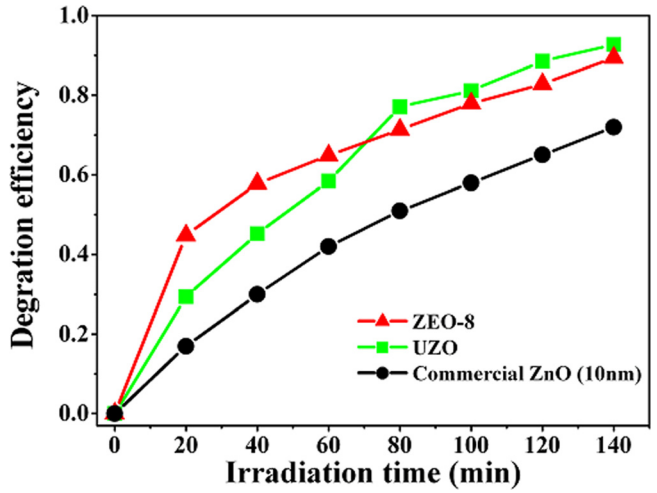

FIG. 10. Degradation efficiency of ZEO-8 for RhB dye versus reaction time.

C. Improved photocatalytic activities

To further explore the functional applications of the graphene-like ZEO, we also characterize their photocatalytic activity on the RhB. Fig. 10 displays the time-dependent RhB degradation efficiency under UV light irradiation in the presence of the UZO, ZEO-8 graphene-like nanosheets, and commercial ZnO nanoparticles. Obviously, the UZO and ZEO-8 exhibit the higher degradation efficiency on the whole compared to the commercial ZnO. The improved photocatalytic activities of the nanosheets demonstrated above can be explained as the synergistic effects of large surface area and improved electron transport ability of charge carriers.[8] On one hand, the large surface area can increase the number of possible reactive sites for adsorbing enough reactant molecules.[8,53–56] On the other hand, both the surface atomic structure and surface area sensitively affect the surface carrier transfer process.[8,53–56] Due to the small thicknesses of UZO and ZEO-8 nanosheets, the charge carriers can be transported very fast once they reach the surface and edge. This improved electron transport ability can substantially suppress the recombination probability of charge carriers in the nanosheets, which strongly improves their photocatalytic reactions. Moreover, it is interesting to note in Fig. 10 that the degradation efficiency of ZEO-8 is higher than that of UZO before exposure to the UV light for 60 min. The incorporation of Eu^{3+} into the ZnO lattices will form trap states to capture photo-generated carriers, which will suppress the carrier recombination and further enhance their photocatalytic activities.[57,58] However, the trap states of Eu^{3+} are limited after all due to the low doping concentration, so that the degradation efficiency of ZEO-8 turns to be same with that of UZO after exposure to the UV light for 60 min.

IV. CONCLUSIONS

In this work, we successfully synthesized the graphene-like Eu^{3+}-doped ZnO nanosheets by a simple hydrothermal

method for the first time as we know. The detailed investigation reveals that the native higher specific surface area has a great influence on the Eu^{3+} red emission and photocatalytic activities. Our results not only provide a candidate material for both flat display and photocatalytic applications but inspire people that the surface effects can be skillfully used to realize or enhance the multi-functional application of nanomaterials.

ACKNOWLEDGMENTS

The authors would like to acknowledge financial support for this work from National Nature Science Foundation of China (Grant Nos. 11204104, 61178074, and 61008051), Program for the Development of Science and Technology of Jilin province (Item Nos. 20110415, 201115219, and 20100113), and program for the Master Students' Scientific and Innovative Research of Jilin Normal University (Item Nos. 201112, 201101, and 201139).

[1]A. Ishizumi and Y. Kanemitsua, Appl. Phys. Lett. **86**, 253106 (2005).
[2]Y. P. Du, Y. W. Zhang, L. D. Sun, and C. H. Yan, J. Phys. Chem. C **112**, 12234 (2008).
[3]D. Wang, G. Xing, M. Gao, L. Yang, J. Yang, and T. Wu, J. Phys. Chem. C **115**, 22729 (2011).
[4]X. Wang, X. Kong, Y. Yu, Y. Sun, and H. Zhang, J. Phys. Chem. C **111**, 15119 (2007).
[5]W. M. Jadwisienczak, H. J. Lozykowski, A. Xu, and B. Patel, J. Electron. Mater. **31**, 776 (2002).
[6]S. S. Ashtaputre, A. Nojima, S. K. Marathe, D. Matsumura, T. Ohta, R. Tiwari, G. K. Dey, and S. K. Kulkarni, J. Phys. D: Appl. Phys. **41**, 015301 (2008).
[7]Y. Zhang, Y. Liu, L. Wu, E. Xie, and J. Chen, J. Phys. D: Appl. Phys. **42**, 085106 (2009).
[8]P. Niu, L. Zhang, G. Liu, and H. M. Cheng, Adv. Funct. Mater. **22**, 4763 (2012).
[9]S. Ithurria, M. D. Tessier, B. Mahler, R. P. S. M. Lobo, B. Dubertret, and Al. L. Efros, Nature Mater. **10**, 936 (2011).
[10]A. K. Geim and K. S. Novoselov, Nature Mater. **6**, 183 (2007).
[11]Y. Omomo, T. Sasaki, L. Z. Wang, and M. Watanabe, J. Am. Chem. Soc. **125**, 3568 (2003).
[12]T. Sasaki, M. Watanabe, H. Hashizume, H. Yamada, and H. Nakazawa, J. Am. Chem. Soc. **118**, 8329 (1996).
[13]J. B. Cui and M. A. Thomas, J. Appl. Phys. **106**, 033518 (2009).
[14]T. Schmidt, K. Lischka, and W. Zulehner, Phys. Rev. B **45**, 8989–8994 (1992).
[15]C. Netzel, V. Hoffmann, T. Wernicke, A. Knauer, M. Weyers, M. Kneissl, and N. Szabo, J. Appl. Phys. **107**, 033510 (2010).
[16]X. Y. Fan, Y. X. Wang, Y. L. Zhang, and L. K. Zeng, J. Synth. Cryst. **37**, 1166 (2008).
[17]J. Lin, J. C. Yu, D. Lo, and S. K. Lam, J. Catal. **183**, 368 (1999).
[18]Y. S. Liu, W. Q. Luo, R. F. Li, G. K. Liu, M. R. Antonio, and X. Y. Chen, J. Phys. Chem. C **112**, 686 (2008).
[19]D. Wei, Y. Liu, Y. Wang, H. Zhang, L. Huang, and G. Yu, Nano Lett. **9**, 1752 (2009).
[20]M. Yoonessi, Y. Shi, D. A. Scheiman, M. Lebron-Colon, D. M. Tigelaar, R. A. Weiss, and M. A. Meador, ACS Nano **6**, 7644 (2012).
[21]L. L. Yang, Q. X. Zhao, M. Willander, X. J. Liu, M. Fahlman, and J. H. Yang, Appl. Surf. Sci. **256**, 3592 (2010).
[22]E. De la Rosa, S. Seplveda-Guzman, B. Reeja-Jayan, A. Torres, P. Salas, N. Elizondo, and M. Jose Yacaman, J. Phys. Chem. C **111**, 8489 (2007).
[23]H. H. Wang, S. H. Baek, J. J. Song, J. H. Lee, and S. W. Lim, Nanotechnology **19**, 075607 (2008).
[24]A. Toumiat, S. Achour, A. Harabi, N. Tabet, M. Boumaour, and M. Maallemi, Nanotechnology **17**, 658 (2006).
[25]X. L. Tan, X. K. Wang, H. Geckeis, and T. H. Rabung, Environ. Sci. Technol. **42**, 6532 (2008).
[26]R. Vercaemst, D. Poelman, L. Fiermans, R. L. Van Meirhaeghe, W. H. Laflere, and F. J. Cardon, J. Electron Spectrosc. Relat. Phenom. **74**, 45 (1995).
[27]A. van Dijken, E. Meulenkamp, D. Vanmaekelbergh, and A. Meijerink, J. Phys. Chem. B **104**, 1715 (2000).
[28]A. Wood, M. Giersig, M. Hilgendorff, A. V. Campos, L. M. Lizmarzan, and P. Mulvaney, Aust. J. Chem. **56**, 1051 (2003).
[29]X. Sui, Y. Liu, C. Shao, Y. Liu, and C. Xu, Chem. Phys. Lett. **424**, 340 (2006).
[30]Y. C. Liu, X. T. Zhang, J. Y. Zhang, Y. M. Lu, X. G. Kong, D. Z. Shen, and X. W. Fan, Chin. J. Lumin. **23**, 563 (2002).
[31]Y. Chen, N. T. Tuan, Y. Segawa, H. Ko, S. Hong, and T. Yao, Appl. Phys. Lett. **78**, 1469 (2001).
[32]W. I. Park, S. J. An, G. C. Yi, and H. M. Jang, J. Mater. Res. **16**, 1358 (2001).
[33]B. P. Zhang, N. T. Binh, K. Wakatsuki, Y. Segawa, Y. Kashiwaba, and K. Haga, Nanotechnology **15**, S382 (2004).
[34]K. Maejima, M. Ueda, S. Fujita, and S. Fujita, Jpn. J. Appl. Phys., Part 1 **42**, 2600 (2003).
[35]Q. X. Zhao, M. Willander, R. E. Morjan, Q. H. Hu, and E. E. B. Campbell, Appl. Phys. Lett. **83**, 165 (2003).
[36]W. I. Park, Y. H. Jun, S. W. Jung, and G. C. Yi, Appl. Phys. Lett. **82**, 964 (2003).
[37]L. L. Yang, Q. X. Zhao, M. Willander, J. H. Yang, and I. Ivanov, J. Appl. Phys. **105**, 053503 (2009).
[38]T. Heinzel, *Mesoscopic Electronics in Solid State Nanostructures* (Wiley-VCH, 2007), p. 76.
[39]I. Shalish, H. Temkin, and V. Narayanamurti, Phys. Rev. B **69**, 245401 (2004).
[40]J. D. Ye, S. L. Gu, F. Gin, S. M. Zhu, S. M. Liu, X. Zhou, W. Liu, L. Q. Hu, R. Zhang, Y. Shi, and Y. D. Zheng, Appl. Phys. A **81**, 759 (2005).
[41]X. L. Wu, G. G. Siu, C. L. Fu, and H. C. Ong, Appl. Phys. Lett. **78**, 2285 (2001).
[42]B. Lin, Z. Fu, and Y. Jia, Appl. Phys. Lett. **79**, 943 (2001).
[43]Z. M. Liao, K. J. Liu, J. M. Zhang, J. Xu, and D. P. Yu, Phys. Lett. A **367**, 207 (2007).
[44]Z. M. Liao, H. Z. Zhang, Y. B. Zhou, J. Xu, J. M. Zhang, and D. P. Yu, Phys. Lett. A **372**, 4505 (2008).
[45]K. Vanheusden, W. L. Warren, C. H. Seager, D. R. Tallant, and J. A. Voigt, J. Appl. Phys. **79**, 7983 (1996).
[46]X. Y. Zeng, J. L. Yuan, and L. D. Zhang, J. Phys. Chem. C **112**, 3503 (2008).
[47]M. Dejneka, E. Snitzer, and R. E. Riman, J. Lumin. **65**, 227 (1995).
[48]K. Ebisawa, T. Okuno, and K. Abe, Jpn. J. Appl. Phys. **47**, 7236 (2008).
[49]D. Nie, T. Xue, Y. Zhang, and X. Li, Sci. China, Ser. B: Chem. **51**, 823 (2008).
[50]B. Cheng, Z. Zhang, H. Liu, Z. Han, Y. Xiao, and S. Lei, J. Mater. Chem. **20**, 7821 (2010).
[51]B. Cheng, Z. Han, H. Guo, S. Lin, Z. Zhang, Y. Xiao, and S. Lei, J. Appl. Phys. **108**, 014309 (2010).
[52]L. L. Yang, Q. X. Zhao, M. Q. Israr, J. R. Sadaf, M. Willander, G. Pozina, and J. H. Yang, J. Appl. Phys. **108**, 103513 (2010).
[53]W. Zhou, F. Sun, K. Pan, G. Tian, B. Jiang, Z. Ren, C. Tian, and H. Fu, Adv. Funct. Mater. **21**, 1922 (2011).
[54]L. Zheng, Y. Zheng, C. Chen, Y. Zhan, X. Lin, Q. Zheng, K. Wei, and J. Zhu, Inorg. Chem. **48**, 1819 (2009).
[55]X. Y. Li, L. H. Chen, Y. Li, J. C. Rooke, C. Wang, Y. Lu, A. Krief, X. Y. Yang, and B. L. Su, J. Colloid Interface Sci. **368**, 128 (2012).
[56]X. Zhang, S. Xu, and G. Han, Mater. Lett. **63**, 1761 (2009).
[57]H. Huang, S. Tian, J. Xu, Z. Xie, D. Zeng, D. Chen, and G. Shen, Nanotechnology **23**, 105502 (2012).
[58]H. Hidaka, T. Shimura, K. Ajisaka, S. Horikoshi, J. Zhao, and N. Serpone, J. Photochem. Photobiol., A **109**, 165 (1997).